Naval Research Laboratory

Washington, DC 20375-5320

NRL/MR/6110--12-9385

Magnetometer Response of Commonly Found Munitions Items and Munitions Surrogates

T.H. Bell
N. Khadr

SAIC, Inc. - ASAD
Arlington, Virginia

G.R. Harbaugh
D.A. Steinhurst

Nova Research, Inc.
Alexandria, Virginia

January 12, 2012

REPORT DOCUMENTATION PAGE

Form Approved
OMB No. 0704-0188

1. REPORT DATE *(DD-MM-YYYY)*	**2. REPORT TYPE**	**3. DATES COVERED** *(From - To)*
12-01-2012	Memorandum Report	January 2010 – September 2011

4. TITLE AND SUBTITLE

Magnetometer Response of Commonly Found Munitions Items and Munitions Surrogates

5a. CONTRACT NUMBER
N00173-05-C-2063

5b. GRANT NUMBER

5c. PROGRAM ELEMENT NUMBER
0603851D8Z

6. AUTHOR(S)

T.H. Bell,* N. Khadr,* G.R. Harbaugh,† and D.A. Steinhurst†

5d. PROJECT NUMBER
MR-1165

5e. TASK NUMBER

5f. WORK UNIT NUMBER
61-5802-A-1-5

7. PERFORMING ORGANIZATION NAME(S) AND ADDRESS(ES)

Naval Research Laboratory, Code 6110
4555 Overlook Avenue, SW
Washington, DC 20375-5320

8. PERFORMING ORGANIZATION REPORT NUMBER

NRL/MR/6110--12-9385

9. SPONSORING / MONITORING AGENCY NAME(S) AND ADDRESS(ES)

Environmental Security Technology Certification Program (ESTCP) Program Office
901 North Stuart Street, Suite 303
Arlington, VA 22203

10. SPONSOR / MONITOR'S ACRONYM(S)
ESTCP

11. SPONSOR / MONITOR'S REPORT NUMBER(S)

12. DISTRIBUTION / AVAILABILITY STATEMENT

Approved for public release; distribution is unlimited.

13. SUPPLEMENTARY NOTES

*SAIC, Inc. - ASAD, 4001 N. Fairfax Drive, 4th Floor, Arlington, VA 22203
†Nova Research, Inc., 1900 Elkin Street, Suite 230, Alexandria, VA 22308

14. ABSTRACT

Target response coefficients for several commonly encountered munitions types and three munitions surrogates were calculated from measurements made using the Naval Research Laboratory Multi-sensor Towed Array Detection System (MTADS) magnetometer array. A best-practice method for making these measurements is presented. Results are presented for four locations in the continental United States: Welcome, MD; Black Hills Army Depot, SD; Hawthorne Army Depot, NV; and a site in Withlacoochee, FL. The minimum-response curves are different for each site because the orientation and strength of the Earth's magnetic field are different at each site. Response curves from Welcome, MD site are shown with corroborative field measurements data overplotted to demonstrate the validity of the method. The results for the large munitions surrogate are the worst fit and this is most likely due to limited ability to degauss large, thick-walled items with available degaussers. Maximum response curves are not presented in this work.

15. SUBJECT TERMS

Unexploded Ordnance (UXO) Munitions Surrogates
Magnetometer

16. SECURITY CLASSIFICATION OF:			**17. LIMITATION OF ABSTRACT**	**18. NUMBER OF PAGES**	**19a. NAME OF RESPONSIBLE PERSON**
a. REPORT	**b. ABSTRACT**	**c. THIS PAGE**			B.J. Spargo, NRL, Code 6110
Unclassified	Unclassified	Unclassified	UU	31	**19b. TELEPHONE NUMBER** *(include area code)* (202) 404-6392

Standard Form 298 (Rev. 8-98)
Prescribed by ANSI Std. Z39.18

This page intentionally left blank

CONTENTS

FIGURES

TABLES

This page intentionally left blank.

ABSTRACT

Target response coefficients for several commonly encountered munitions types and three munitions surrogates were calculated from measurements made using the Naval Research Laboratory Multi-sensor Towed Array Detection System (MTADS) magnetometer array. A best-practice method for making these measurements is presented. Using a magnetically-degaussed (at least modestly) example object, the item is measured oriented horizontal E/W (magnetic). One factor to note in particular is that the peak positive magnetic anomaly is not directly over the item, but positioned off to the south of the item. Information is provided to calculate the proper location to measure the response as a function of sensor height. The scaling of the peak amplitude is related to the angle of the Earth's magnetic field. Scaling is provided for three additional sites and details on how to calculate the scaling for new sites is presented. While it is possible to generate a maximum response curve as well, any remanent magnetization causes more problems for the maximum response curve than the minimum response curve. Maximum response curves are not presented in this work.

Minimum response curves are tabulated for several commonly encountered munitions types and three munitions surrogates. Results are presented for four locations in the continental United States: Welcome, MD; Black Hills Army Depot, SD; Hawthorne Army Depot, NV; and a site in Withlacoochee, FL. The curves are different for each site because the orientation and strength of the Earth's magnetic field are different at each site. Response curves from the Welcome, MD site are shown with corroborative field measurements data overplotted to demonstrate the validity of the method. The results for the large munitions surrogate are the worst fit and this is most likely due to limited ability to degauss large, thick-walled items with available degaussers.

ACKNOWLEDGEMENTS

This work was done as part of NRL's ESTCP-funded participation in 2011 Munitions Response Live Site Demonstrations. The authors would like to thank Craig Murray of Parsons and Stephen Billings of Sky Research for their thoughtful discussions on the subject.

This page intentionally left blank.

MAGNETOMETER RESPONSE OF COMMONLY FOUND MUNITIONS ITEMS AND MUNITIONS SURROGATES

INTRODUCTION

Total-field magnetometer has been a widely-used geophysical sensor for unexploded ordnance (UXO) detection surveys. Recently, electromagnetic induction (EMI) sensors, such as the Geonics, Ltd. EM61-MK2 have seen greater deployment throughout the industry. In areas of benign geology, the total-field magnetometer still finds utility based on its greater depth-of-detection, ease of use, and speed of operation.

In a typical UXO detection survey, the sensor is used to survey the field in a raster pattern with line spacing on the order of the ride height of the sensor above the ground. The magnetometer can be mounted in a variety of airborne and towed arrays, smaller man-portable carts, or carried individually. Smaller line spacing can be used to increase the data density for more advanced analyses. After data collection, the raw data are typically leveled, background corrected, and mapped. Then, either line-by-line or from a data image, regions of anomalous response are selected and marked as potential ferrous metal targets. This initial list of anomalies is used as input to an analysis step that selects anomalies for digging based on features extracted during further analyses such as target size and depth.

There are two schools of thought on how best to select anomalies for the initial list. The goal, of course, is to remove all hazardous objects from the field so one would like to ensure that the initial list includes all hazardous objects. The first approach is to select all points with sensor readings above some multiple of the peak-to-peak background noise floor as anomalies. In some cases, this threshold can be as low as 1.5x the background noise floor, which can lead to a long anomaly list. This approach is intended to maximize the likelihood that all items of interest (unexploded ordnance and residual high explosive material in this case) are included on the anomaly list. By definition, however, it includes a number of items with low signal-to-noise ratio (SNR). In the case described above, this would correspond to an SNR ≈ 4. It is difficult to extract usable target features from signals with such low SNR. So, even if there is a subsequent analysis and classification step, one will often not be able to remove these targets from the dig list, and the items will have to be dug. The average cost of a dig on a munitions site can be up to $125 when the cost of the trained personnel and safety procedures required is factored in. So, the approach that maximizes the number of initial anomalies selected with low SNR can lead to a very expensive remediation; often more than the available resources.

Another approach, which we and others have advocated [1,2], is to consider the possible sensor response of the targets of interest when setting the threshold for anomaly selection. In this approach, one would model the anomaly strength expected for each of the targets of interest and set the threshold at the smallest sensor reading expected from the smallest target of interest at its maximum depth. The term 'anomaly strength' is used here rather than 'signal' to indicate that it is assumed that the mean Earth's magnetic field has been removed from the total-field measurement, yielding a measure of the magnetic anomaly. Even with a safety factor applied to the sensor reading specified above, this method often leads to a higher anomaly selection threshold than the traditional approach. The implication of this is that anomalies due to potential metal objects are left un-remediated but we are confident that the objects

Manuscript approved November 14, 2011.

responsible for the anomaly have a smaller response than any of our targets of interest. This approach to anomaly selection was used at recent Environmental Security Technology Certification Program (ESTCP) UXO Classification Studies [3,4]. At the former Camp Sibert, AL, no targets of interest were missed using this approach.

To implement this target-of-interest based threshold method one must be able to confidently predict the sensor response of all possible items of interest as a function of depth. Over the past ten years we have been involved in a number of programs supported by ESTCP in which we have collected data using Cesium (Cs)-vapor, total-field magnetometers, developed models to interpret those data, and participated in blind tests to validate our procedures.

In this report, we use these models to predict the response of a total-field magnetometer to a number of common munitions items and munitions surrogates as a function of depth. To validate the results, we have collected survey data over these same objects at varying depths and orientations, extracted the maximum anomaly strength observed, and compared the measurements to our predictions. In all cases, the model accurately predicts the measured anomaly amplitudes. After a brief description of the model employed and the data collection methodology, we present the predicted and measured anomaly data in graphical and tabular form. The information provided here applies to a total-field magnetometer.

CS-VAPOR, TOTAL-FIELD MAGNETOMETER

The sensor used in this study is the Geometrics, Inc. G-822ROV/A Cs-vapor magnetometer, but the results are equally applicable to any other total-field magnetometer. The G-822A magnetometers employ an optically pumped Cs-vapor atomic magnetic resonance system that functions as the frequency control element in an oscillator circuit [5]. The frequency of the magnetometer electrical oscillator, or Larmor frequency, varies directly with the ambient magnetic field at the sensor. The accurate measurement of the Larmor frequency therefore provides a precise measurement of the local magnetic field of the Earth. The Earth's magnetic field interacts with ferrous objects, inducing localized anomalies in the measured magnetic field.

The G-822A magnetometer produces a Larmor frequency output at 3.49872 Hz per nT. At the earth's surface, in a nominal 50,000 nT field, the Larmor frequency is about 175 kHz. The G-822A operates over the earth's magnetic field range of 20,000 to 100,000 nT. The Geometrics Supercounter provides 4 channels of counting circuitry to collect data from G-822A sensors . The Larmor frequency output of each magnetometer is converted to local magnetic field (nT) and output via a serial data link to the data acquisition computer (DAQ), where the measurements are time-stamped and recorded.

NRL MTADS MAGNETOMETER ARRAY

The MTADS has been developed by the NRL Chemistry Division with support from ESTCP. The MTADS hardware consists of a low-magnetic-signature vehicle that is used to tow the different sensor arrays over large areas (10 - 25 acres / day) to detect buried UXO. The MTADS tow vehicle and magnetometer array at a recent demonstration site are shown in Figure 1.

Figure 1 – MTADS tow vehicle and magnetometer array.

The MTADS magnetometer array is a linear array of eight Cs-vapor magnetometer sensors (Geometrics, Inc., G-822ROV/A). The sensors are sampled at 50 Hz with a pair of frequency counters (Geometrics, Inc., SuperCounter) and typical surveys are conducted at 6 mph. This results in a sampling density of ~6 cm down track with a cross track sensor spacing of 25 cm. The sensors are nominally mounted 30 cm above the ground. The sensor boom is designed to move up to protect the sensors from damage due to impact with obstructions. This degree of freedom allows some variation in sensor height due to surface roughness. Each magnetometer measures the local magnetic field of the earth at the sensor.

Typically, a single GPS antenna placed directly above the center of the sensor array is used to measure the sensor positions in real-time (5 Hz). For situations that require it, such as on the steep hill shown in Figure 1, a pair of GPS antennae can be mounted above the magnetometers in a manner similar to that used on the AMTADS platform [6] to provide array yaw and roll information. All navigation and sensor data are time-stamped with Universal Coordinated Time (UTC) derived from the satellite clocks and recorded by the DAQ in the tow vehicle. The DAQ runs the MagLogNT software package (v2.921b, Geometrics, Inc.) and the data streams from each device are recorded in separate files with a common root filename.

COMMONLY FOUND MUNITIONS

Seven of the commonly found UXO items previously studied [1] with the Geonics EM61-MK2 were studied. Pictures of each item can be found in the Results section.

MUNITIONS SURROGATES

Three munitions surrogates previously studied [2] with the Geonics EM61-MK2 were studied. In selecting a useful munitions surrogate, one might choose items which are widely available, inexpensive, and unlikely to cause excitement if found by non-study participants. In this case, we have chosen to use standard pipe nipples. Each of the three surrogates employed is a black, welded steel, Schedule 40 straight pipe nipple, threaded on both ends. We obtained the samples for this study on-line from McMaster-Carr (http://www.mcmaster.com/) but they are widely available from a variety of sources. The details of the three surrogates are given in Table 1.

Table 1 – Munitions surrogates used in this work.

Item	Nominal Pipe Size	Outside Diameter	Length	Part Number
Small Surrogate	1"	1.315" (33.4 mm)	4"	44615K466
Medium Surrogate	2"	2.375" (60.3 mm)	8"	44615K529
Large Surrogate	4"	4.500" (114.3 mm)	12"	44615K137

METHOD FOR DETERMINING RESPONSE CURVES

Response curves describe how the peak magnetic anomaly strength of an object varies with the depth and orientation of the object. The magnetic anomaly from a steel object depends on the strength and orientation of the magnetization of the object, which in turn depend on the size and shape of the object, its orientation relative to the geomagnetic field, the geomagnetic field strength, and any residual or remanent magnetization in the object. When the remanent magnetization is negligible (e.g. if the object has been degaussed), the weakest anomalies occur when the object is aligned perpendicular to the geomagnetic field. This is the least favorable geometry for detection because the anomaly strengths are weakest. The simplest weak-anomaly geometry has the object horizontal, pointing east/west. This is illustrated in Figure 2. The anomaly peak does not occur directly above the target. It is offset to the south by a distance that is proportional to the sensor height above the target and depends on the geomagnetic dip angle as shown in the plot on the right. The proportionality factor is tabulated for geomagnetic dip angles in one degree increments below (Table 2).

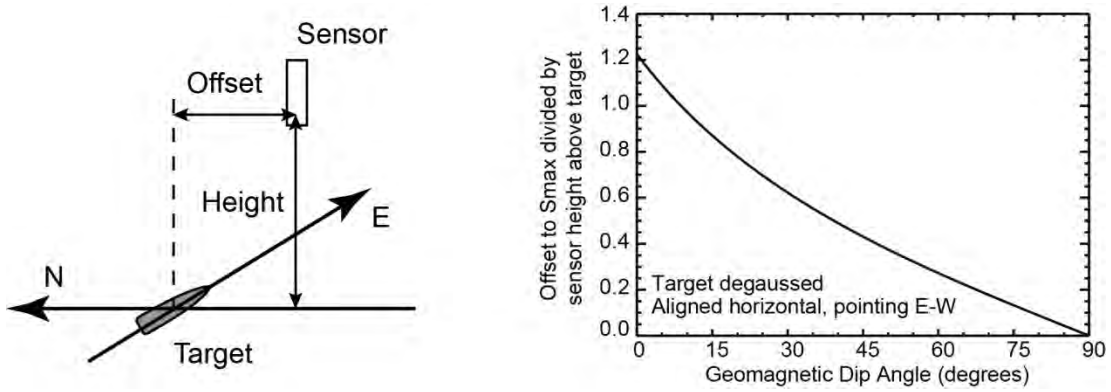

Figure 2 – Diagram on the left shows the weak-anomaly geometry with horizontal target aligned east/west. The anomaly peak is offset from the position directly over target by an amount shown in the plot on the right.

Table 2 – Offset to anomaly peak as fraction of sensor height above target.

Dip	Offset	Dip	Offset	Dip	Offset	Dip	Offset	Dip	Offset	Dip	Offset
0	1.225	16	0.852	32	0.594	48	0.398	64	0.234	80	0.088
1	1.196	17	0.833	33	0.581	49	0.387	65	0.224	81	0.079
2	1.168	18	0.815	34	0.567	50	0.376	66	0.215	82	0.070
3	1.141	19	0.797	35	0.554	51	0.365	67	0.206	83	0.061
4	1.115	20	0.779	36	0.541	52	0.354	68	0.196	84	0.052
5	1.090	21	0.762	37	0.528	53	0.344	69	0.187	85	0.044
6	1.065	22	0.746	38	0.515	54	0.333	70	0.178	86	0.035
7	1.041	23	0.729	39	0.503	55	0.323	71	0.169	87	0.026
8	1.018	24	0.713	40	0.491	56	0.313	72	0.159	88	0.017
9	0.995	25	0.697	41	0.478	57	0.303	73	0.150	89	0.009
10	0.973	26	0.682	42	0.466	58	0.293	74	0.141	90	0.000
11	0.952	27	0.667	43	0.455	59	0.283	75	0.132		
12	0.931	28	0.652	44	0.443	60	0.273	76	0.123		
13	0.910	29	0.637	45	0.431	61	0.263	77	0.114		
14	0.890	30	0.623	46	0.420	62	0.253	78	0.105		
15	0.871	31	0.608	47	0.409	63	0.243	79	0.097		

The weak or worst-case response curve for a target can be constructed from measurements of the peak target anomaly strength at several distances below the sensor with the target horizontal, pointing east/west. The anomaly peaks are measured at the offset distances corresponding to the sensor height above the target determined from the plot in Figure 2 or from Table 2. The anomaly strength will then vary inversely as the third power of sensor height above the target, and the appropriate scale factor can be determined by fitting such a curve through the measured peak anomaly strength values. Figure 3 shows examples of response curves and peak magnetic anomaly strengths for several targets as measured using the MTADS magnetometer array. Targets were oriented east-west (weakest anomaly strengths), north-south (intermediate anomaly strengths), and vertically (strongest anomaly strengths). The solid lines show the weak or worst case response. Dashed lines are fit to the data for vertically oriented targets.

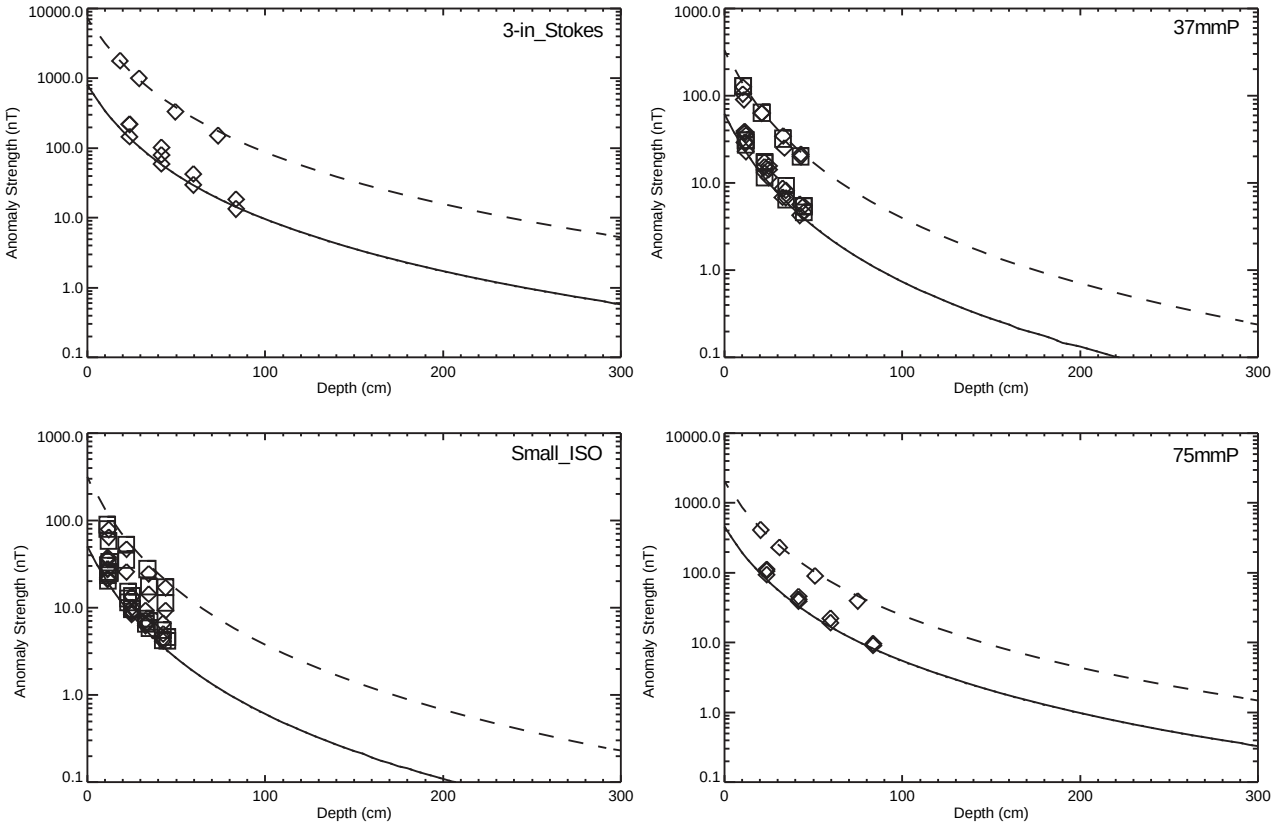

Figure 3 – Examples of response curves. Solid lines are weak or worst case response curves corresponding to horizontal, east/west target orientation. Dashed lines show response curves fitted to data collected with target vertical.

DATA COLLECTION PROCEDURES

Each item was carefully degaussed for several cycles using an audio tape degausser (Audio Lab, Model TD-5-115-60). Data collection was carried out for each of the munitions items and munitions surrogates studied.

While it is possible to generate a response curve by making single, static measurements at each depth / orientation for a given munition using the position indicated in Figure 2 and Table 2, it was more practical for us to use the MTADS magnetometer array. The data from a single pass of the sensor array at normal survey speed over the object, starting ten meters in front of the pit and continuing ten meters past the pit, were collected for each depth / orientation pair. Before and after each series of measurements, data were collected over the empty pit to ensure that the sensor background was at reasonable levels. The survey data were background corrected using data collected before and after the test pit and the peak positive amplitude anomaly strength selected. A magnetometer survey was conducted over each of the test objects positioned at a variety of depths and orientations in our test pit at Blossom Point. As discussed above, the peak location is not necessarily located directly above the object. Each object was measured at multiple unique position / orientation pairs.

SCALING RESPONSE CURVES FOR OTHER LOCATIONS

The minimum response for an ordnance item scales with the strength of the geomagnetic field and with a factor that depends on the dip angle. Figure 4 and Table 3 show the scale factor $F(\theta)$ as functions of the dip angle θ. If the anomaly strength at some location A is S_A, then the corresponding anomaly strength at a different location B (S_B) is given by

$$S_B = H_B F(\theta_B) S_A / H_A F(\theta_A)$$

where H_A and H_B are the geomagnetic field strengths at A and B, and θ_A and θ_B are the corresponding geomagnetic dip angles.

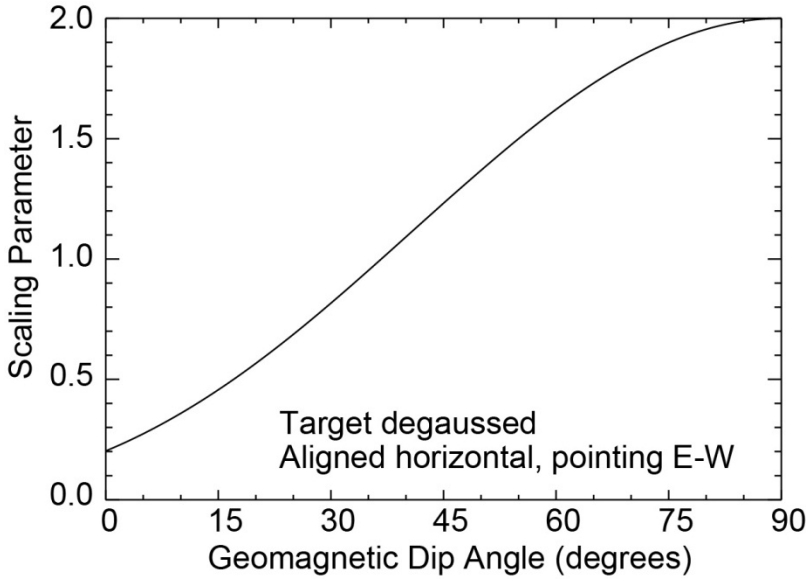

Figure 4 – Scaling Parameter as a Function of Geomagnetic Dip Angle

Table 3 – Scaling parameter as a function of geomagnetic dip angle

Dip	Scale	Dip	Scale	Dip	Scale	Dip	Scale	Dip	Scale	Dip	Scale
0	0.202	16	0.478	32	0.870	48	1.315	64	1.710	80	1.955
1	0.216	17	0.499	33	0.897	49	1.342	65	1.730	81	1.963
2	0.229	18	0.521	34	0.925	50	1.369	66	1.750	82	1.971
3	0.244	19	0.544	35	0.952	51	1.396	67	1.770	83	1.978
4	0.259	20	0.566	36	0.980	52	1.422	68	1.788	84	1.984
5	0.274	21	0.590	37	1.008	53	1.448	69	1.807	85	1.989
6	0.290	22	0.614	38	1.036	54	1.474	70	1.824	86	1.993
7	0.306	23	0.638	39	1.064	55	1.500	71	1.840	87	1.996
8	0.323	24	0.662	40	1.092	56	1.525	72	1.856	88	1.998
9	0.341	25	0.687	41	1.120	57	1.550	73	1.871	89	2.000
10	0.359	26	0.712	42	1.148	58	1.574	74	1.886	90	2.000
11	0.377	27	0.738	43	1.176	59	1.598	75	1.899		
12	0.396	28	0.764	44	1.204	60	1.621	76	1.912		
13	0.416	29	0.790	45	1.232	61	1.644	77	1.924		
14	0.436	30	0.817	46	1.260	62	1.667	78	1.935		
15	0.456	31	0.843	47	1.287	63	1.689	79	1.945		

RESULTS

The results of this investigation are shown in Figure 5 through Figure 14. For each of the figures, the top panel is a photograph of the actual item measured and the bottom panel shows the predicted and measured magnetometer response. The response is plotted as 'anomaly strength' which is in the units of nT and indicates that the values are background-subtracted. The predicted response when the item is in its least favorable orientation is plotted as a solid line. Measured responses are plotted as open circles. In all cases, the measured responses are described well by the calculated curves. All predicted sensor responses are tabulated in a spreadsheet which is attached electronically as Appendix A.

The minimum magnetometer anomaly strengths predicted for all the targets investigated at a single depth are excerpted from Appendix A in Table 4. A depth below the surface corresponding to 11x an object's diameter is often the *de facto* expectation for detectability with modern geophysical equipment. It is the anomaly strength at this depth that can be used as the basis for an anomaly selection threshold. In the ESTCP Classification Pilot Program [7] at the former Camp Sibert, AL, such a threshold was used with a safety margin of 50%. Unlike the EM61-MK2, there is no ready-defined 'standard' configuration to reference, so all other data and plots in this document express depth as the distance below the active area of the sensor to the center of the target. For Table 4, two depths are reported, the "Depth Below Sensor" and the "11x Depth," which factors in the ride height of the MTADS array used to collect the data (30 cm).

The site-specific background magnetometer anomaly strength, which limits the ultimate depth of detection of the item under investigation, was determined at the site. The RMS noise at this site is typically 2 nT but this is a strong function of the roughness of the terrain and may be higher at other sites.

The test pit at Blossom Point is only a little deeper than 1 m. Thus, for the larger objects we were unable to make measurements down to this 11x depth. This has no practical effect as the predicted responses are well validated by the data collected down to 1 m.

Table 4 – Predicted minimum magnetometer anomaly strength for a variety of munitions and surrogate items at a burial depth corresponding to 11x their respective diameter. The sensor is assumed to be deployed as part of the NRL MTADS system at a ride height of 30 cm above the ground. The presented values are for the Earth's magnetic field at our facility in Welcome, MD. The depth below sensor is also provided.

Item	Depth Below Sensor (m)	11x Depth (m)	Minimum Anomaly Strength at 11x Depth (nT)
81-mm mortar	1.19	0.89	8.6
3-in Stokes mortar	1.14	0.84	13.9
75-mm projectile	1.13	0.83	8.1
2.75-in rocket warhead	1.07	0.77	12.7
40-mm grenade	0.74	0.44	2.3
37-mm projectile	0.71	0.41	4.4
Hand Grenade	0.91	0.61	3.1
Large Munitions Surrogate	1.56	1.26	13.7
Medium Munitions Surrogate	0.96	0.66	8.7
Small Munitions Surrogate	0.67	0.37	4.3

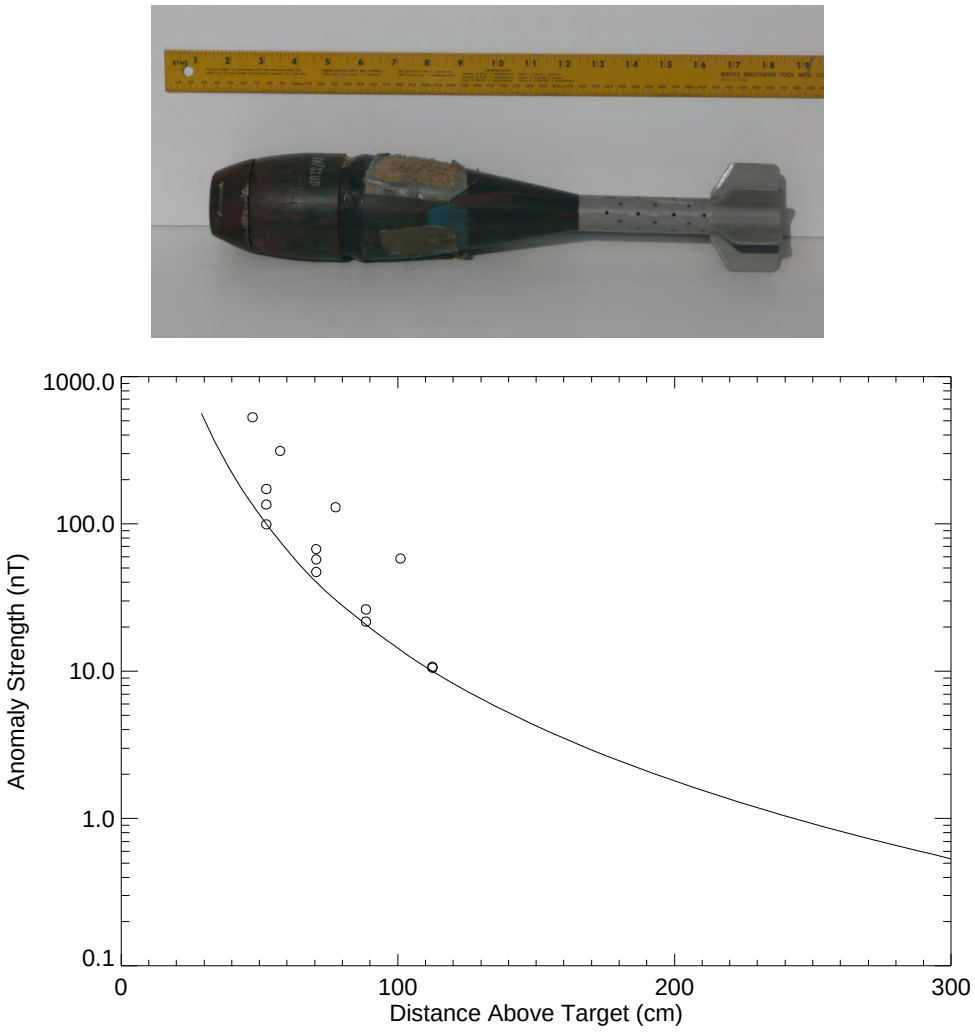

Figure 5 – Peak magnetometer anomaly strength as a function of the distance of the center of an 81-mm mortar below the sensor's active area. The predicted response to the object in its least favorable orientation is shown as a solid line, test pit measurements are plotted as open circles.

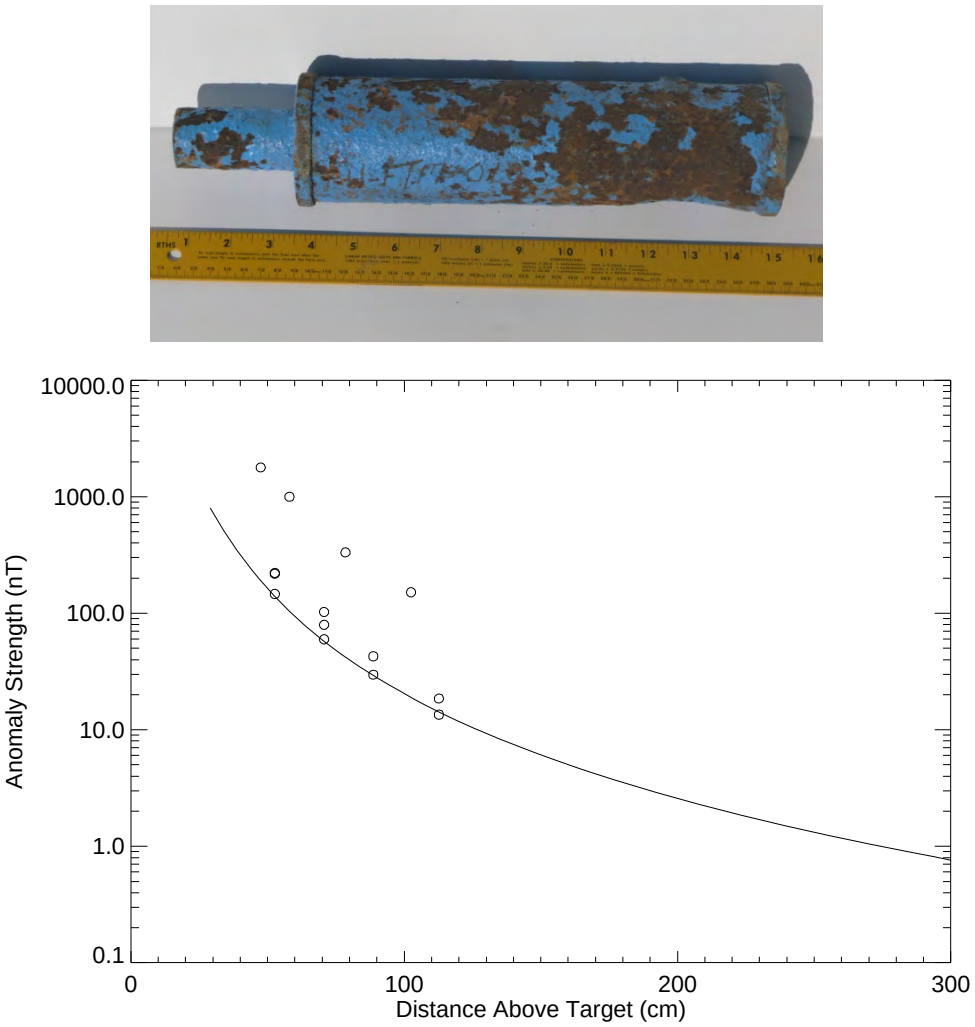

Figure 6 – Peak magnetometer anomaly strength as a function of the distance of the center of a 3-in Stokes mortar below the sensor's active area. The predicted response to the object in its least favorable orientation is shown as a solid line, test pit measurements are plotted as open circles.

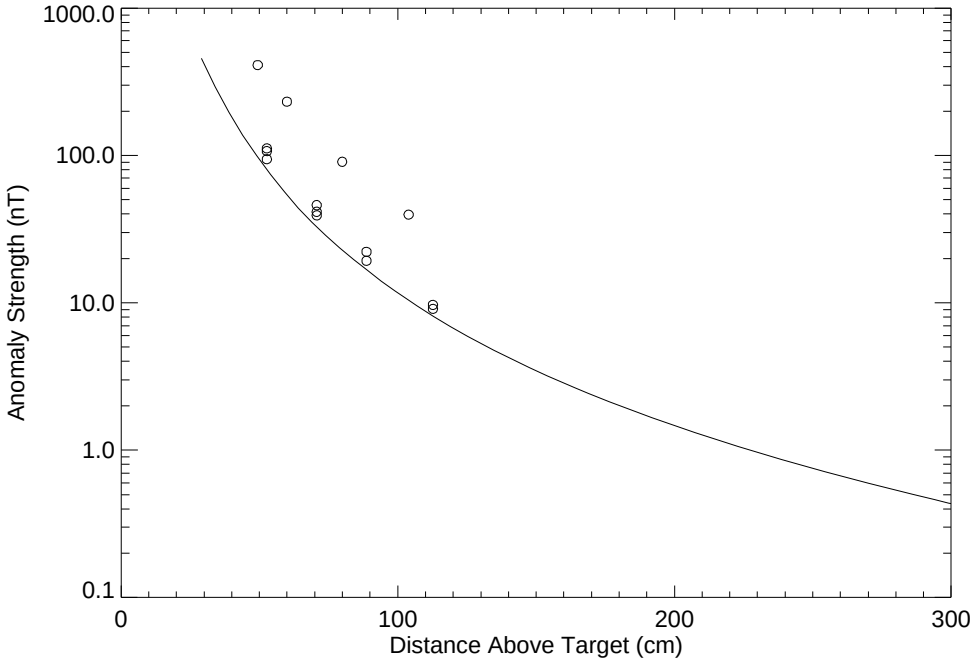

Figure 7 – Peak magnetometer anomaly strength as a function of the distance of the center of a 75-mm projectile below the sensor's active area. The predicted response to the object in its least favorable orientation is shown as a solid line, test pit measurements are plotted as open circles.

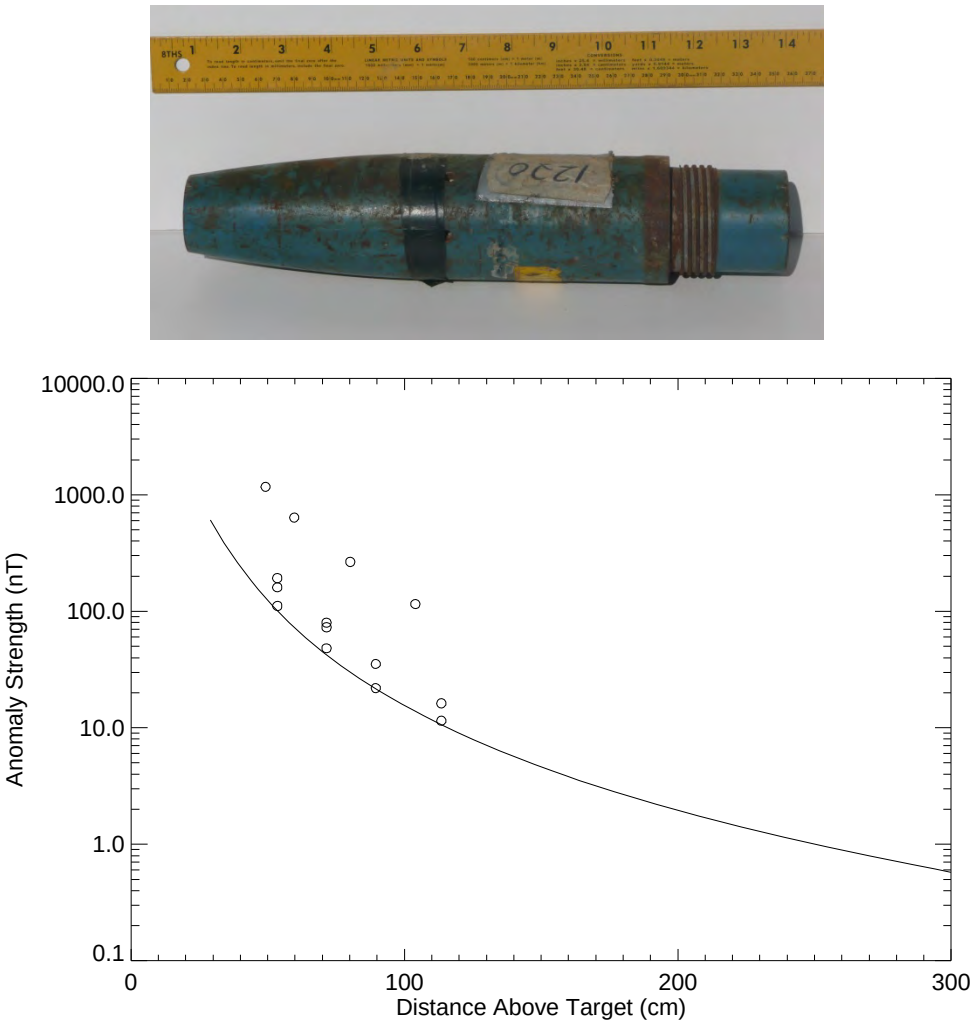

Figure 8 – Peak magnetometer anomaly strength as a function of the distance of the center of a 2.75-in rocket warhead below the sensor's active area. The predicted response to the object in its least favorable orientation is shown as a solid line, test pit measurements are plotted as open circles.

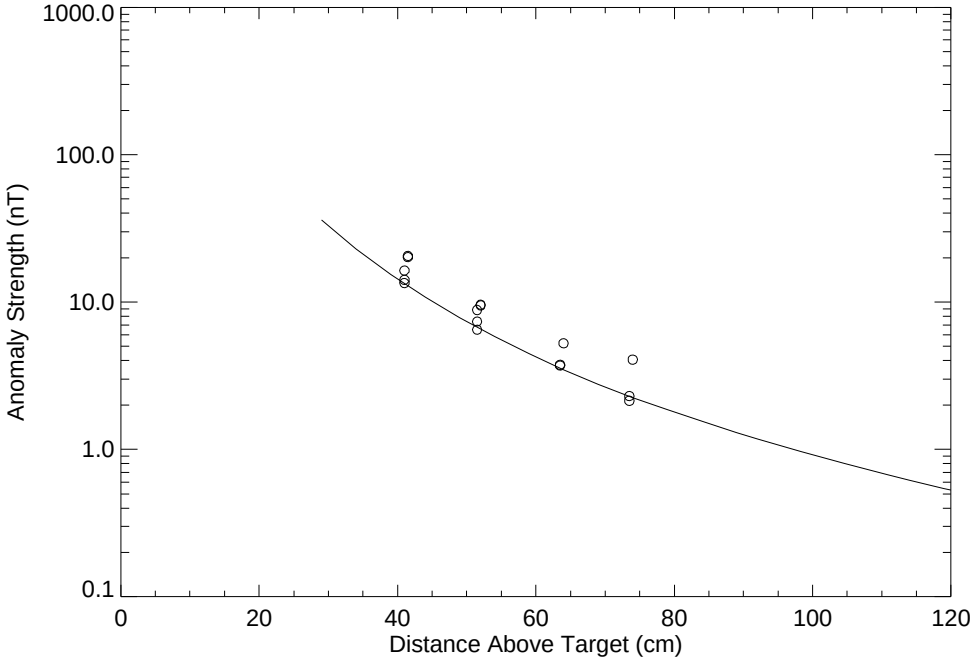

Figure 9 – Peak magnetometer anomaly strength as a function of the distance of the center of a 40-mm grenade below the sensor's active area. The predicted response to the object in its least favorable orientation is shown as a solid line, test pit measurements are plotted as open circles.

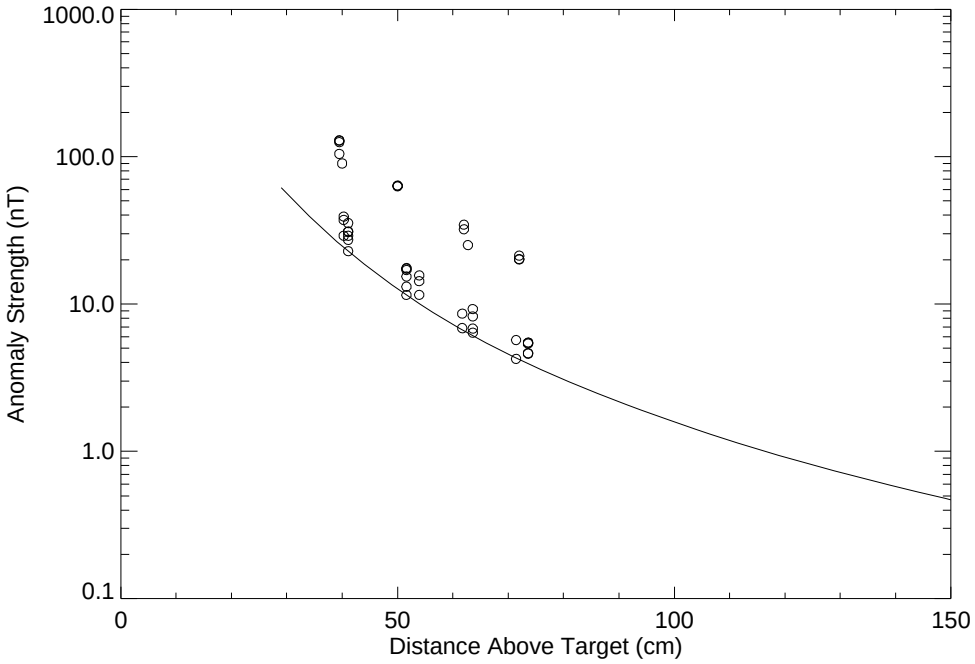

Figure 10 – Peak magnetometer anomaly strength as a function of the distance of the center of a 37-mm projectile below the sensor's active area. The predicted response to the object in its least favorable orientation is shown as a solid line, test pit measurements are plotted as open circles.

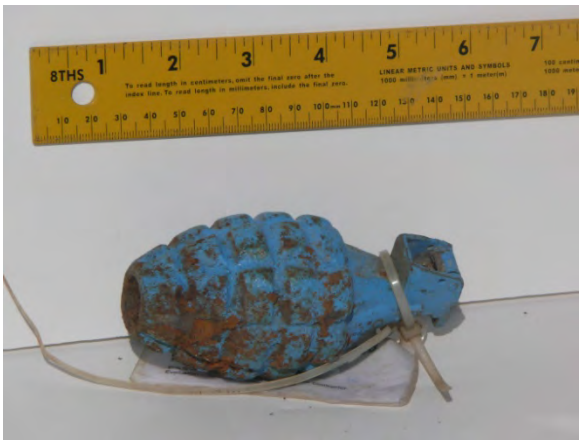

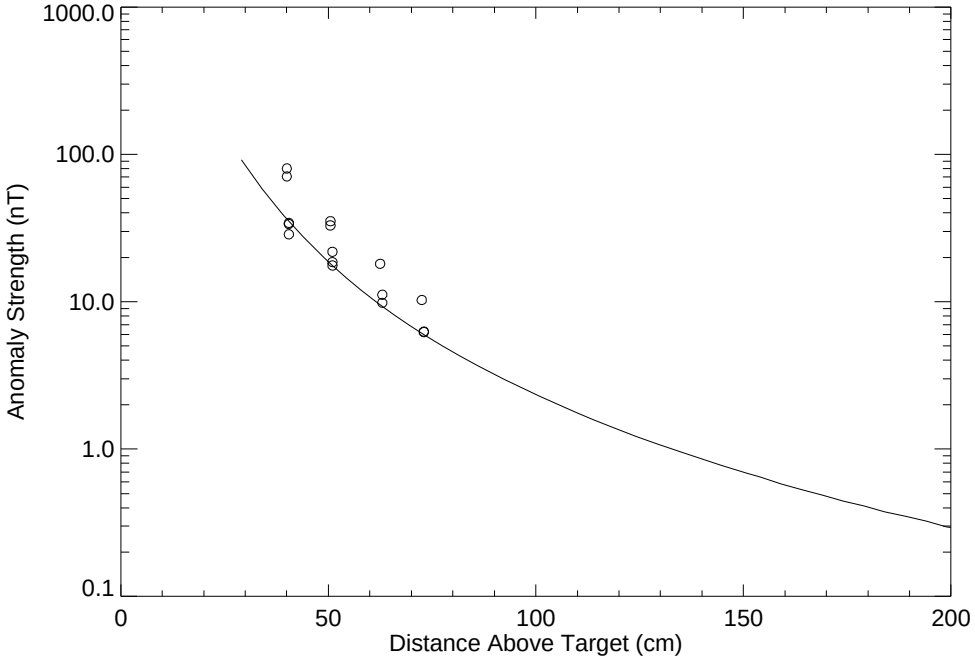

Figure 11 – Peak magnetometer anomaly strength as a function of the distance of the center of a hand grenade below the sensor's active area. The predicted response to the object in its least favorable orientation is shown as a solid line, test pit measurements are plotted as open circles.

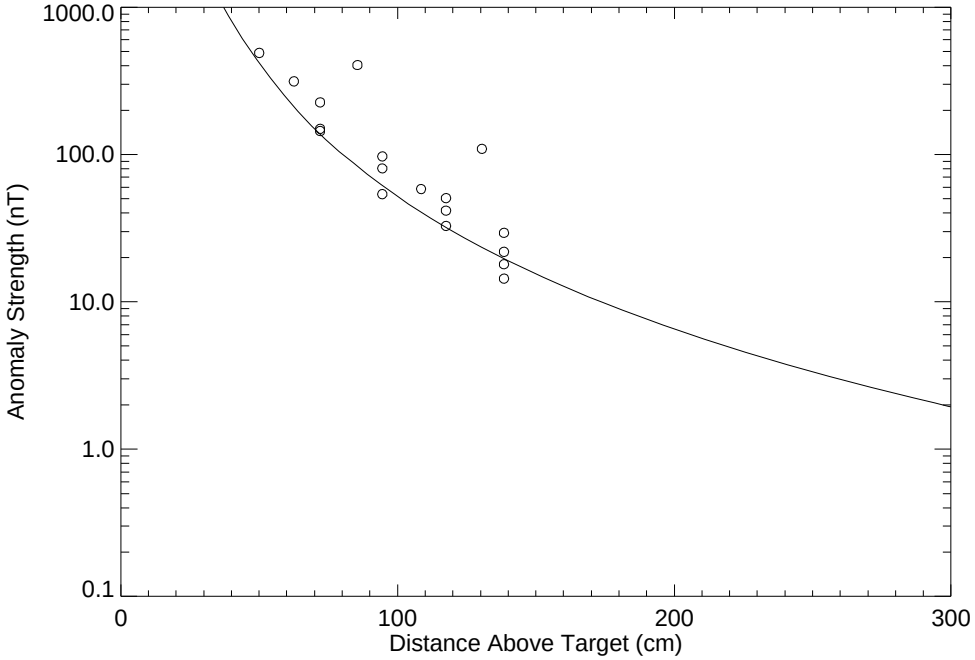

Figure 12 – Peak magnetometer anomaly strength as a function of the distance of the center of a large munitions surrogate below the sensor's active area. The predicted response to the object in its least favorable orientation is shown as a solid line, test pit measurements are plotted as open circles.

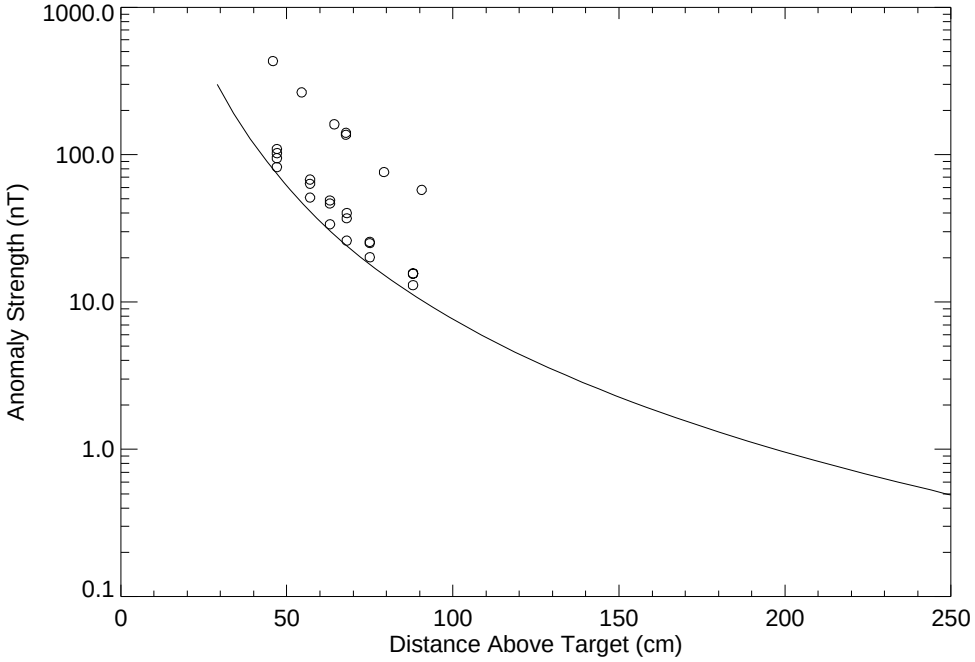

Figure 13 – Peak magnetometer anomaly strength as a function of the distance of the center of a medium munitions surrogate below the sensor's active area. The predicted response to the object in its least favorable orientation is shown as a solid line, test pit measurements are plotted as open circles.

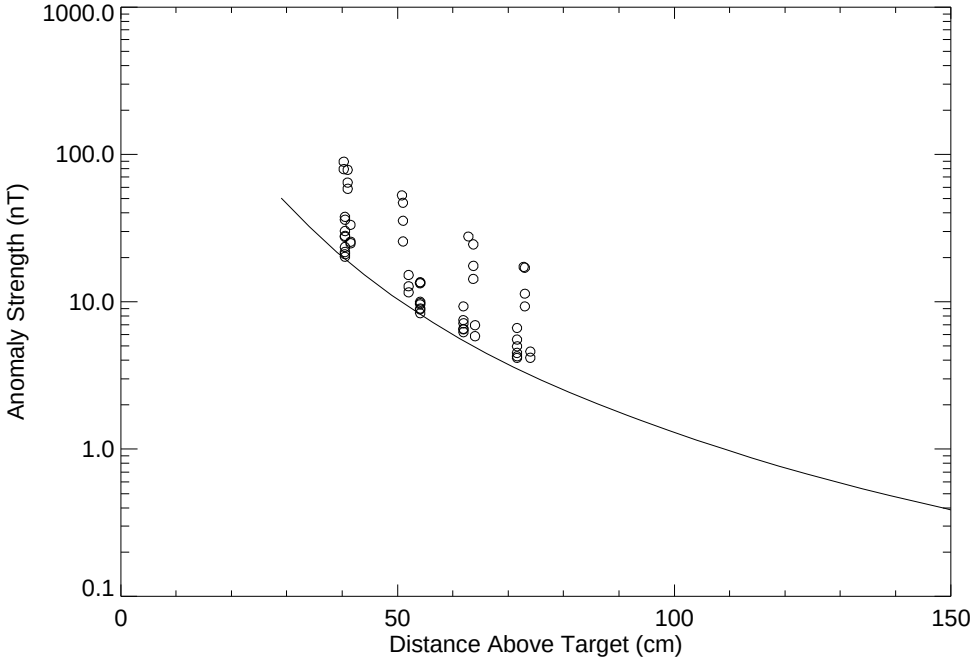

Figure 14 – Peak magnetometer anomaly strength as a function of the distance of the center of a small munitions surrogate below the sensor's active area. The predicted response to the object in its least favorable orientation is shown as a solid line, test pit measurements are plotted as open circles.

SUMMARY

We have used the NRL MTADS Magnetometer Array to characterize a number of inert munitions items commonly found on Military Munitions Response Sites and example surrogate items. Using these data we have determined magnetometer response coefficients for each object at our test facility in Welcome, MD. These response coefficients have been used to calculate the expected anomaly strength from a cesium magnetometer over each object as a function of depth. These results have been presented graphically and the minimum anomaly strength expected at a depth corresponding to 11x the objects diameter has been tabulated. As the Earth's magnetic field varies with location, tabulated parameters are provided for predictive purposes at other locations. The response coefficients for three other locations in the continental United States are presented in the appendix. A mathematical procedure for translating these results to additional sites is discussed.

REFERENCES

1. "EM61-MK2 Response of Standard Munitions Items," Nelson, H.H., Bell, T., Kingdon, J., Khadr, N., Steinhurst, D.A., NRL Memorandum Report NRL/MR/6110—08-9155, Naval Research Laboratory, Washington, DC, 20375, October 6, 2008. http://serdp-estcp.org/content/download/8454/103959/file/Munitions%20Report-MR_9155.pdf

2. "EM61-MK2 Response of Three Munitions Surrogates," H.H. Nelson, T. Bell, J. Kingdon, N. Khadr, D.A. Steinhurst, NRL Memorandum Report NRL/MR/6110--090-9183, Naval Research Laboratory, Washington, DC, March 12, 2009. http://serdp-estcp.org/content/download/8453/103951/file/ISO%20Report-MR_9183.pdf

3. Harbaugh, G. R., Steinhurst, D. A., and Khadr, N. "MTADS Demonstration at Camp Sibert Magnetometer / EM61 MkII / GEM-3 Arrays," Demonstration Data Report, August 21, 2008. http://serdp-estcp.org/content/download/5614/77761/file/MM-0533-GEM-Data.pdf

4. "ESTCP Pilot Program, Classification Approaches in Munitions Response, San Luis Obispo, California, Final Report", H.H Nelson, K. Kaye, A. Andrews, May, 2010. http://serdp-estcp.org/content/download/7424/94825/file/ESTCP-Classification-CampSLO-Final-Report-26May2010.pdf

5. "Operation Manual, G-822A and G-823A & B CESIUM MAGNETOMETER, 27597-OM REV. B," Geometrics, Inc., 2004. ftp://geom.geometrics.com/pub/mag/Manuals/MAN822AO_revB5.pdf

6. "MTADS Magnetometer Survey of the Badlands Bombing Range, SD Impact Area, Combined Airborne, Vehicular, and Man-portable Survey, September 2002," H.H. Nelson, D.A. Steinhurst, D. Wright, T. Furuya, J.R. McDonald, B. Barrow, N. Khadr, and J. Haliscak, NRL/MR-MM/6110—03-8666. http://serdp-estcp.org/content/download/4467/66305/file/MM-4003

7. "ESTCP Pilot Program, Classification Approaches in Munitions Response, Final Report" H.H Nelson, K. Kaye, A. Andrews, November 17, 2008. http://serdp-estcp.org/content/download/7423/94821/version/1/file/ESTCP-Classification-CampSibert-FinalReport+12-17-09.pdf

APPENDIX A – RESPONSE CURVES BY LOCATION

The tabulated data to generate response curves for Cs-vapor total magnetometers at four locations in the continental United States are presented in the electronic version of this Appendix. First, the results used to generate the figures in the main document are presented for our home location in Welcome, MD. Next, the data for three other locations are presented.

Our facility in Welcome, Maryland is located in southern Maryland.

38º 25’ N, 77º 6’ W, 2m (elev.)

Data are also provided for three additional sites:

The Black Hills Army Depot, SD, 43º 15’ N, 103º 45’ W, 1170m (elev.).

Withlacoochee, FL., 28º 32’ N, 82º 03’ W, -30m (elev.).

The Hawthorne Army Depot, NV, 38º 16’ N, 118º 34’ W, 1410m (elev.).